Rare Metal Materials and Engineering
Volume 52, Issue 9, September 2023
Available online at www.rmme.ac.cn

Science Press

Cite this article as: Qin Feng, Shen Zhengyan, Shi Qi, et al. Effect of Processing Parameters on Microstructure and Mechanical Properties of Ta Prepared by Selective Laser Melting[J]. Rare Metal Materials and Engineering, 2023, 52(09): 3026-3036.

ARTICLE

Effect of Processing Parameters on Microstructure and Mechanical Properties of Ta Prepared by Selective Laser Melting

Qin Feng[1,2,3,4], Shen Zhengyan[2,3,4], Shi Qi[2,3,4], Zhou Ge[1], Yao Dao[5], Zhao Yumin[1,2,3,4], Liu Xin[2,3,4], Chen Lijia[1]

[1] School of Materials Science and Engineering, Shenyang University of Technology, Shenyang 110870, China; [2] Institute of New Materials, Guangdong Academy of Sciences, Guangzhou 510650, China; [3] Guangdong Provincial Key Laboratory of Metal Toughening Technology and Application, Guangzhou 510650, China; [4] National Engineering Research Center of Powder Metallurgy of Titanium & Rare Metals, Guangzhou 510650, China; [5] Heyuan Institute of Guangdong Academy of Sciences, Heyuan 517000, China

Abstract: The effects of single-layer and double-layer scanning strategies and energy density (246–640 J/mm^3) on the microstructures and mechanical properties of Ta prepared by selective laser melting (SLM) were investigated. The microstructure of SLM-processed Ta was characterized by scanning electron microscope and electron backscatter diffractometer. The microhardness and tensile properties were also tested. Results show that the Ta microstructure is composed of columnar crystals with obviously upward growth trend and the Ta prepared by double-layer scanning has finer grain size. With increasing the input energy density, the strength, microhardness, and ductility of the as-built Ta are significantly improved. In addition, the double-layer scanning strategy can further improve the densification of Ta specimen, and even increases the ductility without strength loss. When the energy density is 640 J/mm^3 (double-layer scanning), the as-built Ta exhibits optimal properties: the microhardness, ultimate tensile strength, and elongation are 2307 MPa, 527 MPa, and 11.4%, respectively.

Key words: selective laser melting; scanning strategy; mechanical properties; Ta

Ta with melting point of 2996 ° C has been widely employed in aerospace and biomedical industries owing to its excellent corrosion resistance and biocompatibility[1–2]. As a biocompatible material, Ta can easily cause cell adhesion and proliferation. Thus, it is often used as bone replacement implant in the medical field[3–5]. The traditional methods to produce Ta components mainly include the smelting and powder metallurgy processes[6]. Recently, the rapid development in additive manufacturing attracts much attention[7]. As the most promising additive manufacturing technique, selective laser melting (SLM) can produce highly customized parts with thin-wall and hollow structures[8–10]. SLM process contains computer-aided technique, powder transfer, and laser sintering, i. e., SLM is a computer-controlled layer-by-layer laser scanning process of powder, as shown in Fig.1.

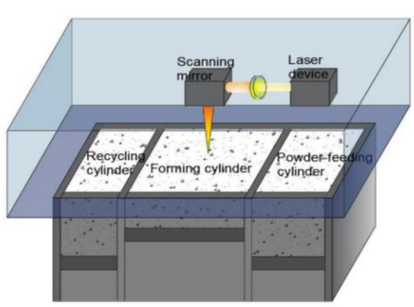

Fig.1 Schematic diagram of SLM process

Received date: January 17, 2023
Foundation item: Key Realm R&D Program of Guangdong Province (2018B090904004); Key Research Program of Guangzhou (202206040001); GDASHY Project of Science and Technology Development (2021GDASHY-0107); Science and Technology Program of Qingyuan (2021DZX028); Guangdong Academy of Science Project of Science and Technology Development (2020GDASYL-20200103142, 2022GDASZH-2022010107)
Corresponding author: Shi Qi, Ph. D., Institute of New Materials, Guangdong Academy of Sciences, Guangzhou 510650, P. R. China, E-mail: shiqi@gdinm.com

The laser processing parameter is an important influence factor to SLM process and to the properties of processed material. It is reported that the appropriate laser energy density, scanning strategy, and substrate preheating temperature can significantly affect the densification, microstructure evolution, and mechanical properties of material through the variation of molten pool[11–13]. Sungail et al[14] investigated the effect of oxygen content and heat treatment on the properties of SLM-processed Ta and found that the decreased oxygen content and a suitable heat treatment (2000 ° C/2 h) can increase the elongation without strength loss. Zhou et al[15] investigated the effects of laser power (150 – 300 W) and scanning speed (60–200 mm/s) on the mechanical properties of SLM-processed Ta, and reported that the microhardness and tensile strength of Ta after SLM process at laser power of 250 W and scanning speed of 100 mm/s increase to 4361 and 739 MPa, respectively. Livescu et al[16] found that different laser energy densities also have significant effect on density, grain size, and grain orientation of Ta. Thijs et al[17] investigated the effect of scanning strategy on the microstructure of Ta metal. It is suggested that rotating the scanning direction between layers can produce higher planar isotropy in the crystal texture and grain shape. It is worth noting that the single-layer and double-layer scanning methods also have significant impact on the properties of SLM-processed Ta materials. Liu et al[18] investigated the effect of double-layer scanning on the microstructure and mechanical properties of $AlSi_{10}Mg$. It is found that the double-layer scanning can refine the grains and increase the density and hardness. Pan et al[19] obtained the 306L material with relative density, surface roughness, ultimate tensile strength, and elongation of 99.31%, 6.67 μm, 725 MPa, and 40.8% through double-layer scanning, respectively. This result indicates that the double-layer scanning strategy can improve the material properties. However, the double-layer scanning strategy is rarely used for pure tantalum.

This research investigated the effects of single-layer and double-layer scanning on the microstructure and mechanical properties of SLM-processed Ta, providing experimental support for the practical application of SLM forming and manufacturing of Ta-based alloys.

1 Experiment

The raw material powder used in this research was spherical Ta powder prepared by radio-frequency plasma spheroidization technique, and its morphology was characterized by SU8220 scanning electron microscope (SEM), as shown in Fig 2. The powder was basically free of satellite particles and only had a few hole defects. The BT-101 metal powder apparent density analyzer, BT301 tap density analyzer, and BT-200 metal powder flowability analyzer were used to measure the apparent density, tap density, and Hall flowability of Ta powder, respectively. The results are shown in Table 1.

The Ta bulk material was fabricated by SLM machine (EOS 100), and the corresponding processing parameters are shown in Table 2. Archimedes method was used to measure the density, and the SU822 high-resolution field emission SEM was used to characterize the microstructure. The specimens used for SEM and electron backscattered diffraction (EBSD) observation were ground by sandpaper of 280#, 500#, 800#, 1000#, and 2000# and then polished by SiO_2 polishing solution for 3 h. EBSD analysis was operated at accelerating voltage of 20 kV, scanning step of 0.5 μm, working distance of 12 mm, and aperture of 120 μm under high current mode. According to GB/T 31930-2015 standard, tensile tests were conducted by DNS200 universal tensile testing machine at speed of 1 mm/min, and the tensile specimen size is shown in Fig.3.

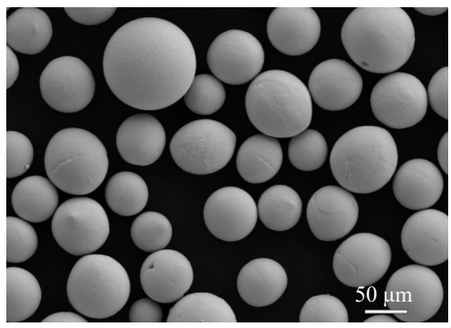

Fig.2 SEM morphology of raw Ta powder

Table 1 Properties of raw Ta powder

Apparent density/g·cm^{-3}	Tap density/ g·cm^{-3}	Hall flowability/ s·(50 g)$^{-1}$	Oxygen content/wt%
9.44	10.49	5.78	0.06

2 Results and Discussion

2.1 Densification

The relative densities of SLM-processed Ta are shown in Fig.4. It can be seen that the relative density of Ta specimens is gradually increased from 95.82% to 98.44% with increasing the energy density from 246 J/mm^3 to 640 J/mm^3. Additionally, the relative density of Ta specimen after SLM process with double-layer scanning at energy density of 246, 457, and 640 J/mm^3 increases to 97.13%, 98.58%, and 98.97%, respectively.

The surface morphologies of SLM-processed Ta are shown in Fig. 5. BD stands for building direction. At energy density of 246 J/mm^3 (Fig. 5a), the unmelted powder and pit defects can be clearly observed on the surface. At energy density of 320 J/mm^3 (Fig. 5b), the spherical spatters with irregular shapes disappear on the surface and the incompletely filled hole defects remain. At energy density of 457 J/mm^3 (Fig.5c), the hole defects are significantly reduced on the Ta specimen surface. At energy density of 640 J/mm^3 (Fig. 5d), the specimen surface presents uniform morphology. Compared with those after single-layer scanning (Fig. 5a and 5c), the surface fusion of Ta specimen after double-layer scanning (Fig.5e and 5f) shows better quality: the pores are significantly reduced,

Table 2 SLM processing parameters

Specimen No.	Laser power/W	Laser speed/ mm·s^{-1}	Hatch space/mm	Layer thickness/mm	Energy density/ J·mm^{-3}	Number of scanning layers
S1	240	650	0.05	0.03	246	1
S2	240	500	0.05	0.03	320	1
S3	240	350	0.05	0.03	457	1
S4	240	250	0.05	0.03	640	1
S5	240	650	0.05	0.03	246	2
S6	240	350	0.05	0.03	457	2
S7	240	250	0.05	0.03	640	2

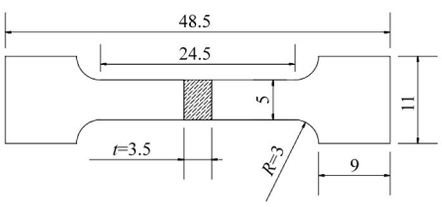

Fig.3 Schematic diagram of Ta tensile specimen

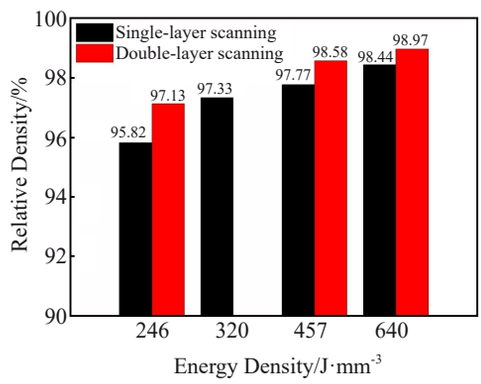

Fig.4 Relative densities of Ta specimens after SLM process at different energy densities

the specimen surface becomes flatter, and the melt pool structure is more obvious.

This is because when the energy density of input laser is low (246 J/mm^3), the large particles can hardly melt, and the high scanning speed can easily cause the splash of powder particles. When the energy density increases to 320 J/mm^3, the large powder particles completely melt, and the high scanning speed leads to the incomplete filling of melt pool as well as the formation of pores. With further increasing the energy density to 457 J/mm^3, the Ta powder completely melt and the slow laser scanning promotes the complete filling of melt pool, thereby reducing the porosity. The energy density of 640 J/mm^3 is sufficient for powder melting and melt pool filling, resulting in good surface morphology. Additionally, the double-layer scanning remelts the metal at the surface, which results in better filling of the melt pool, therefore leading to

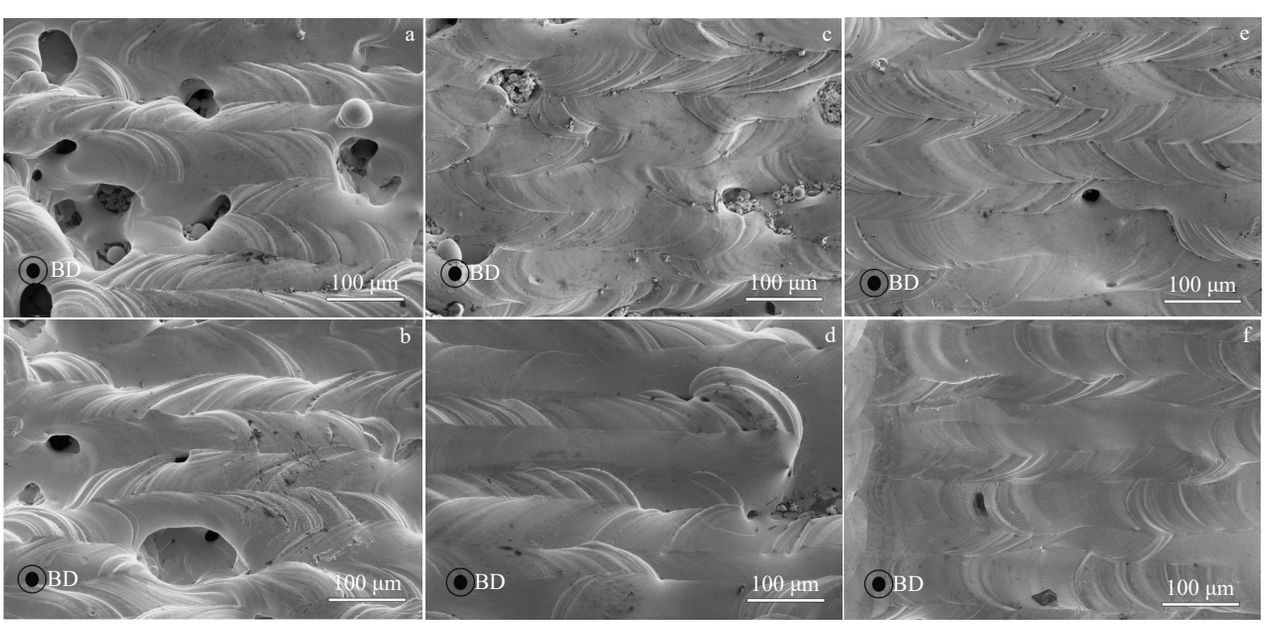

Fig.5 Surface morphologies of Ta specimens after SLM process with single-layer scanning (a–d) and double-layer scanning (e–f) at different energy densities: (a, e) 246 J/mm^3, (b) 320 J/mm^3, (c) 457 J/mm^3, and (d, f) 640 J/mm^3

flatter surface morphology.

The pore distribution of SLM-processed Ta specimens is shown in Fig. 6. At energy density of 246 J/mm^3 (Fig. 6a), the SLM-processed Ta contains a large number of irregular pores and unmelted spherical powder particles. At energy density of 320 J/mm^3 (Fig. 6b), the pores inside the Ta specimen change to laterally arranged strips. At energy density of 457 J/mm^3 (Fig. 6c), the Ta specimen presents irregular pores of smaller size. At energy density of 640 J/mm^3 (Fig. 6d), the Ta specimen has few pores of further smaller size. Additionally, the Ta after SLM process with double-layer scanning barely has hole defects, compared with those after single-layer scanning. The variation of pore distribution of the SLM-processed Ta specimens is consistent with that of specimen density, suggesting that the increase in the energy density and the amelioration in scanning strategy can lead to the reduction in porosity.

Fig. 7 shows the schematic diagrams of SLM processes at different energy densities to explain the relationship between energy density and porosity. The low energy density of 246 J/mm^3 cannot sufficiently melt the powder particles in the melt pool, forming irregular holes. Besides, the powder particles can barely remain in the previously scanned layer (Fig. 7a) for complete melt. When the energy density increases to 320 J/mm^3, the powder particles melt completely in the melt pool, but the liquid metal cannot completely fill the defects at the top scanned layer, thus forming striated holes. With further increasing the energy density to 457 J/mm^3, the liquid metal in the melt pool becomes flatter (Fig. 7c) and the specimen surface has less defects, thus reducing the formation of pores. At energy density of 640 J/mm^3, the holes are greatly reduced due to the good combination between melt pool and substrate.

2.2 Microstructure

The microstructures of Ta specimens after different SLM processes are shown in Fig. 8. It can be seen that the Ta specimens all have similar crystal structures of columnar grains, whose width is 30–100 μm. It is worth noting that the columnar grains in the Ta specimens after double-layer scanning are shorter than those after single-layer scanning. It is found that the SLM-processed specimens tend to form columnar crystals. When a new layer is deposited, the previous layer remelts, and the columnar grains grow up along the thermal gradient at the solid/liquid interface[20]. During the double-layer scanning, due to the higher thermal conductivity and reflectivity of the metallic solid, compared with those of the powder[21], the secondary scanning cannot completely remelt the previously formed melt pool. Therefore, the previously formed melt pool partially remelts, and the top columnar particles remelt, resulting in shorter columnar crystals[18], as shown in Fig.9.

Fig. 10 shows EBSD results of Ta specimens after SLM process with single-layer scanning at different energy densities. These results are consistent with the microstructure observations: the specimen shows a clearly upward growth trend of columnar crystal structures. During SLM process, the molten melt pool solidifies rapidly, and the inhomogeneous nucleation sites in the molten liquid can form equiaxed grains. Additionally, the columnar-to-equiaxed transformation (CET) occurs when the number and size of equiaxed grains are large enough to impede the movement of columnar solid-liquid[22]. However, pure Ta is prone to the formation of columnar crystals due to the lack of structural supercooling and sufficient nucleation sites to interrupt the epitaxial growth[20]. The critical condition for CET process can be expressed by Eq.(1–3), as follows:

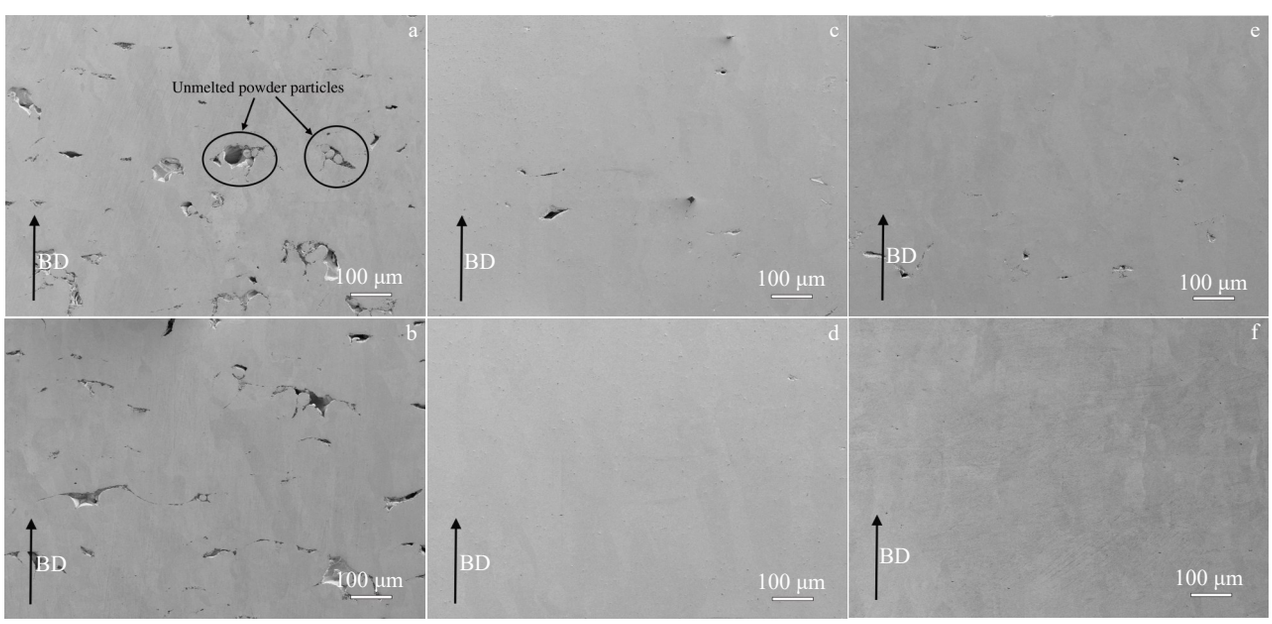

Fig.6 Pore distributions of Ta specimens after SLM process with single-layer scanning (a–d) and double-layer scanning (e–f) at different energy densities: (a, e) 246 J/mm^3, (b) 320 J/mm^3, (c) 457 J/mm^3, and (d, f) 640 J/mm^3

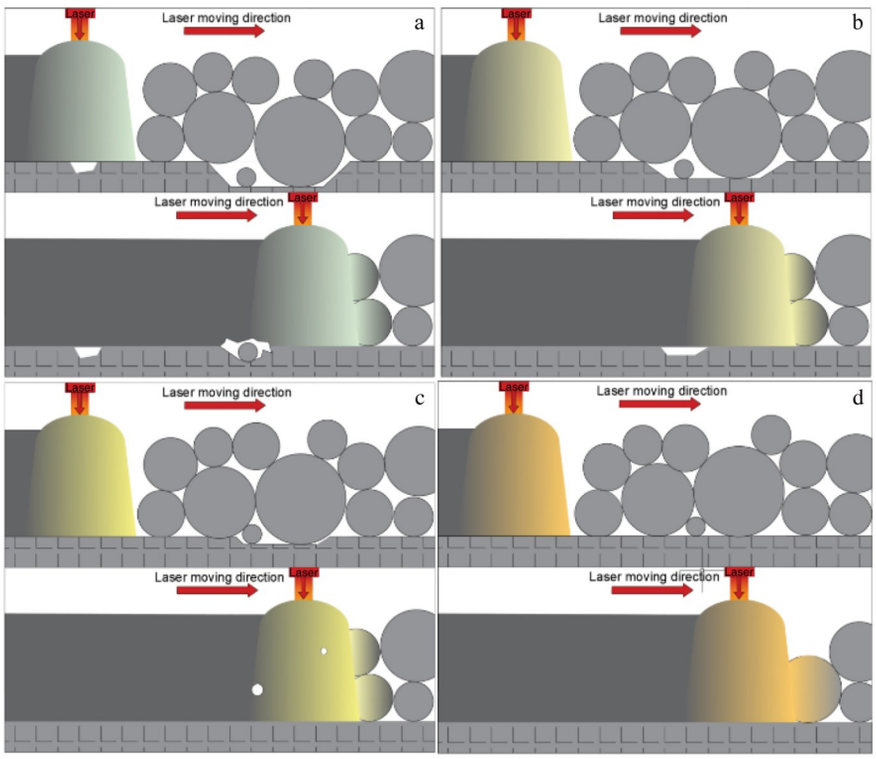

Fig.7 Schematic diagrams of SLM process with single-layer scanning at different energy densities: (a) 246 J/mm^3, (b) 320 J/mm^3, (c) 457 J/mm^3, and (d) 640 J/mm^3

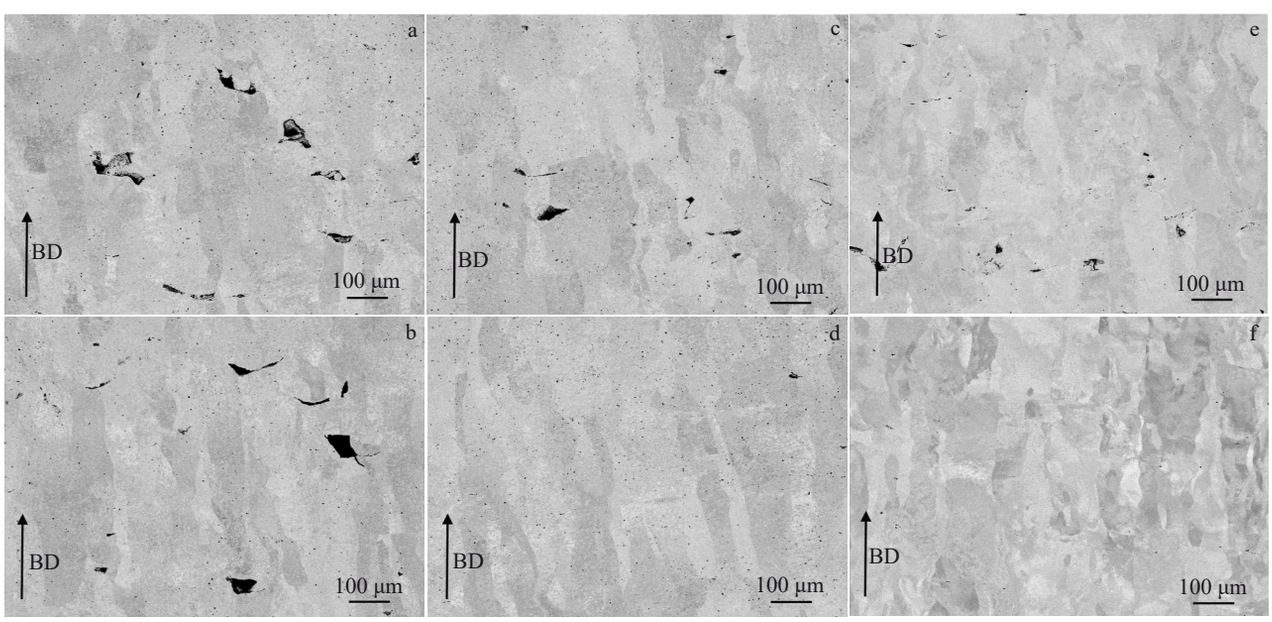

Fig.8 Microstructures of Ta specimens after SLM process with single-layer scanning (a–d) and double-layer scanning (e–f) at different energy densities: (a, e) 246 J/mm^3, (b) 320 J/mm^3, (c) 457 J/mm^3, and (d, f) 640 J/mm^3

$G^n/V>C_{CET}$ columnar grain (1)

$G^n/V>C_{CET}$ transition line (2)

$G^n/V>C_{CET}$ equiaxed grain (3)

where C_{CET} is the critical value of the non-uniform nucleation point, G is the temperature gradient, V is the solidification rate, and n is the metal material parameter[18]. Therefore, the higher the temperature gradient G, the lower the solidification rate V, and the easier the formation of columnar grains. The temperature gradient is an important factor to the grain morphology of SLM-processed metals as well as the initial driving force for solidification, which is along the direction of

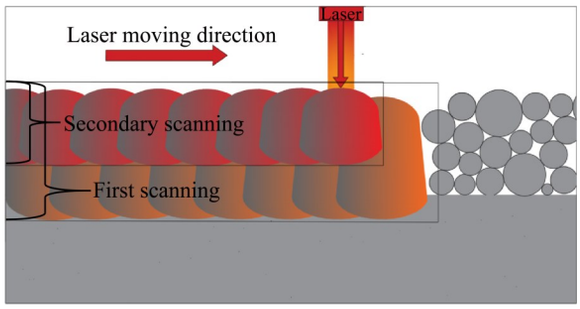

Fig.9 Schematic diagram of SLM process with double-layer scanning strategy

maximum temperature gradient. During SLM process, the laser scanning is conducted layer by layer and the diffusion direction to the upper surface is the optimal heat dissipation path, promoting the grain formation along the upward growth of columnar crystal structure[23–24]. Although the later formed layer has lower temperature gradient and higher solidification rate, which promotes the formation of equiaxed grains, the top of the previously formed layer still melts, leading to the loss of equiaxed grains and the production of fully columnar grain morphology in the final metal parts.

Fig. 11 shows the kernel average misorientation (KAM) of Ta specimens after SLM process with single-layer scanning at different energy densities. KAM shows the local orientation difference of Ta specimen, which qualitatively reflects the homogenization degree of plastic deformation and the density of dislocation accumulation. Thus, KAM can be used to evaluate the material stress distribution during deformation. According to Fig. 11, with increasing the energy density, the dislocation aggregation (red region) is increased obviously. This is mainly due to the thermal impact of each deposited layer on the microstructure of previously solidified layer during the layer-by-layer scanning process. Besides, the cyclic and repetitive thermal effects cause the accumulation of thermal stresses[25]. It is reported that the local strain caused by thermal contraction and expansion in additive manufacturing is 1.7%[26]. Under the combined effect of thermal stress and thermal strain, the specimen is prone to the formation of high-density dislocations inside the structures. In addition, with increasing the energy density, the thermal influence region of each deposited layer is increased, the cyclic thermal effect is improved, the dislocation density is increased. With increasing the dislocation density and degree of freedom, the dislocation cell structure is preferentially formed[27]. The formation of dislocation cell structures ameliorates the movement of multiple slip systems during plastic deformation and promotes the good combination of strength and plasticity[28].

Fig. 12 shows the Schmid factor distributions of Ta specimens after SLM process with single-layer scanning at different energy densities. It can be seen that the Schmid factor of the SLM-processed Ta specimens ranges from 0.3 to 0.5, indicating the good plasticity of SLM-processed Ta specimens. Besides, the Schmid factor is increased with increasing the energy density. The Schmid factor is an important indicator for slip deformation of metal materials, and the calculation formula of Schmid factor is ms=cosφcosλ, where φ and λ represent the angle between the force axis and the normal direction of the slip surface and the angle between the force axis and the slip direction, respectively. The higher the Schmid factor, the higher the initiation probability of slip system, the more the reduction in deformation caused by

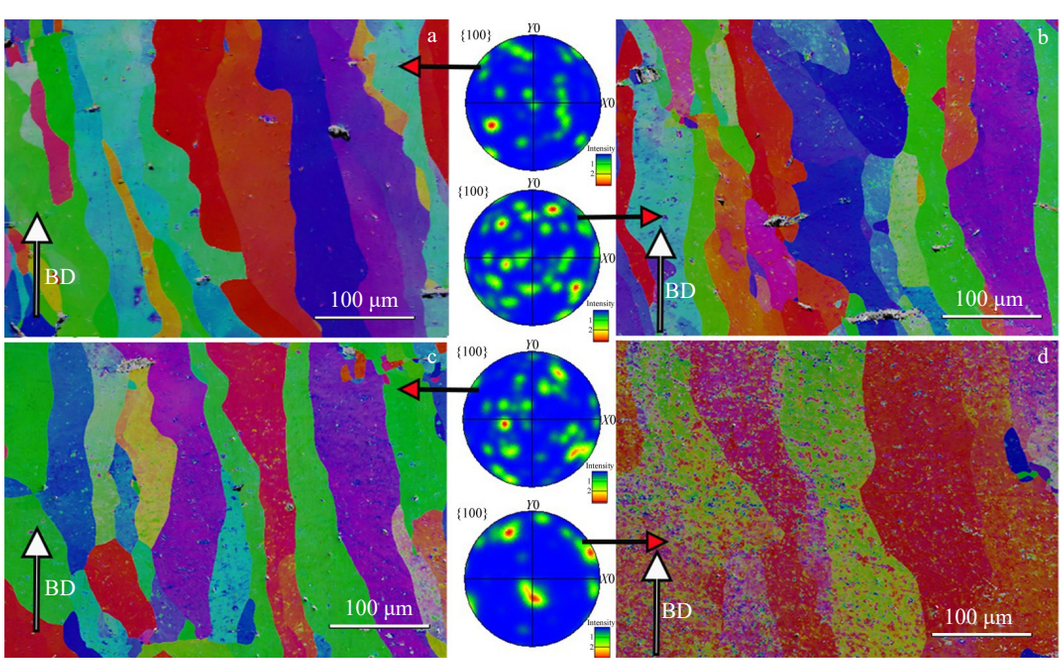

Fig.10 EBSD microstructures of Ta specimens after SLM process with single-layer scanning at different energy densities: (a) 246 J/mm^3, (b) 320 J/mm^3, (c) 457 J/mm^3, and (d) 640 J/mm^3

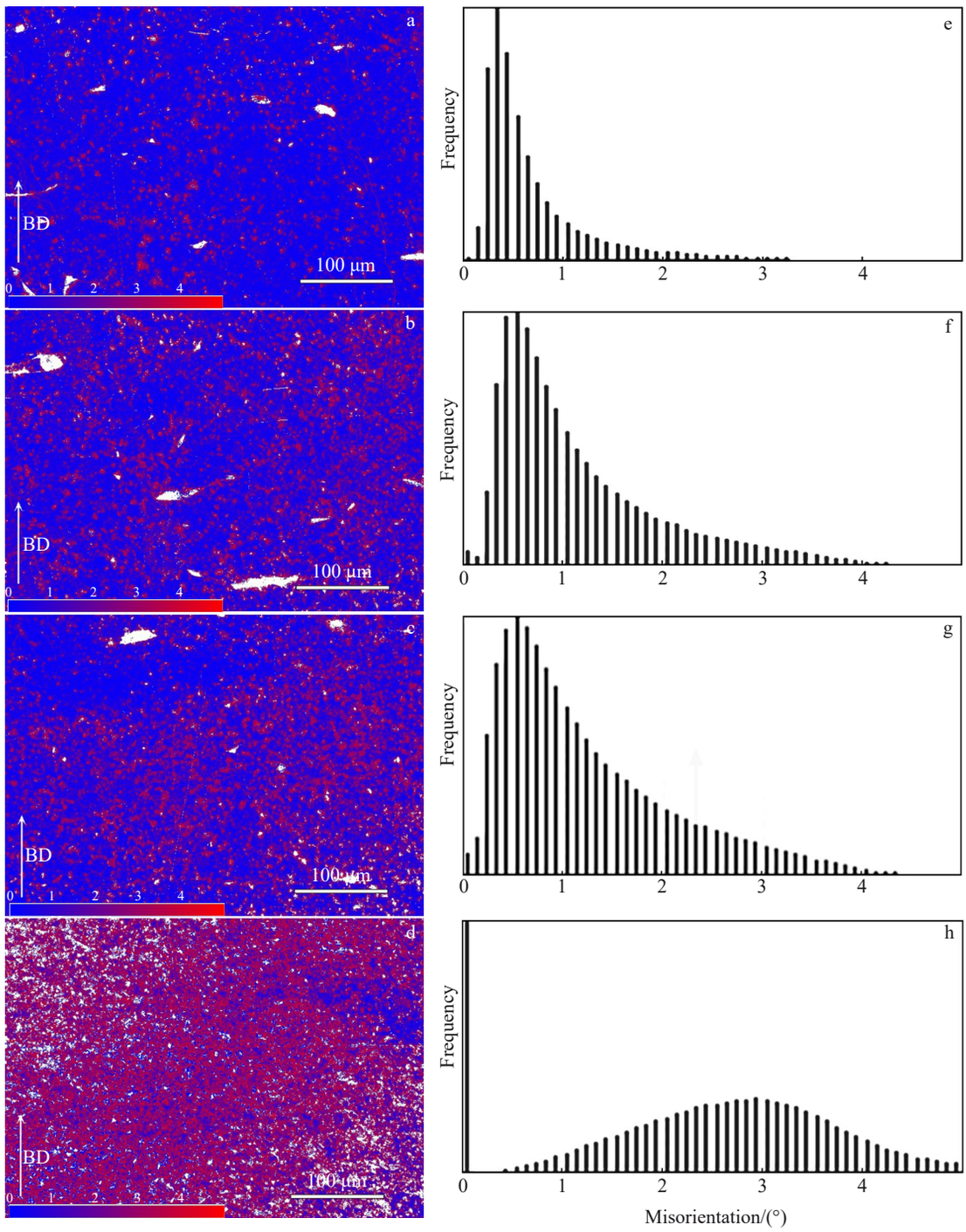

Fig.11 KAMs of Ta specimens after SLM process with single-layer scanning at different energy densities: (a, e) 246 J/mm^3, (b, f) 320 J/mm^3, (c, g) 457 J/mm^3, and (d, h) 640 J/mm^3

stress concentration, and thus the higher the plasticity of material. It is found that the fraction of Schmid factor≥0.46 f(ms≥0.46) is gradually increased from 30% to 31%, 35%, and 70% with increasing the energy density from 246 J/mm^3 to 320, 457, and 640 J/mm^3, respectively. The increase in energy density leads to the higher temperature of melt pool, so the larger temperature gradient occurs at the front edge. Furthermore, the higher energy input results in more dramatic Marangoni convection and more dislocation defects in the grains, thereby increasing the Schmid factor.

2.3 Mechanical properties

The microhardness and ultimate tensile strength of Ta specimens after different SLM processes are shown in Fig. 13 and Fig. 14, respectively, which are significantly higher than those prepared by casting (1078 and 205 MPa) and powder metallurgy (1176 and 310 MPa)[15]. According to Fig. 13, the microhardness of Ta specimens is increased with increasing the energy density, and the double-layer scanning strategy can

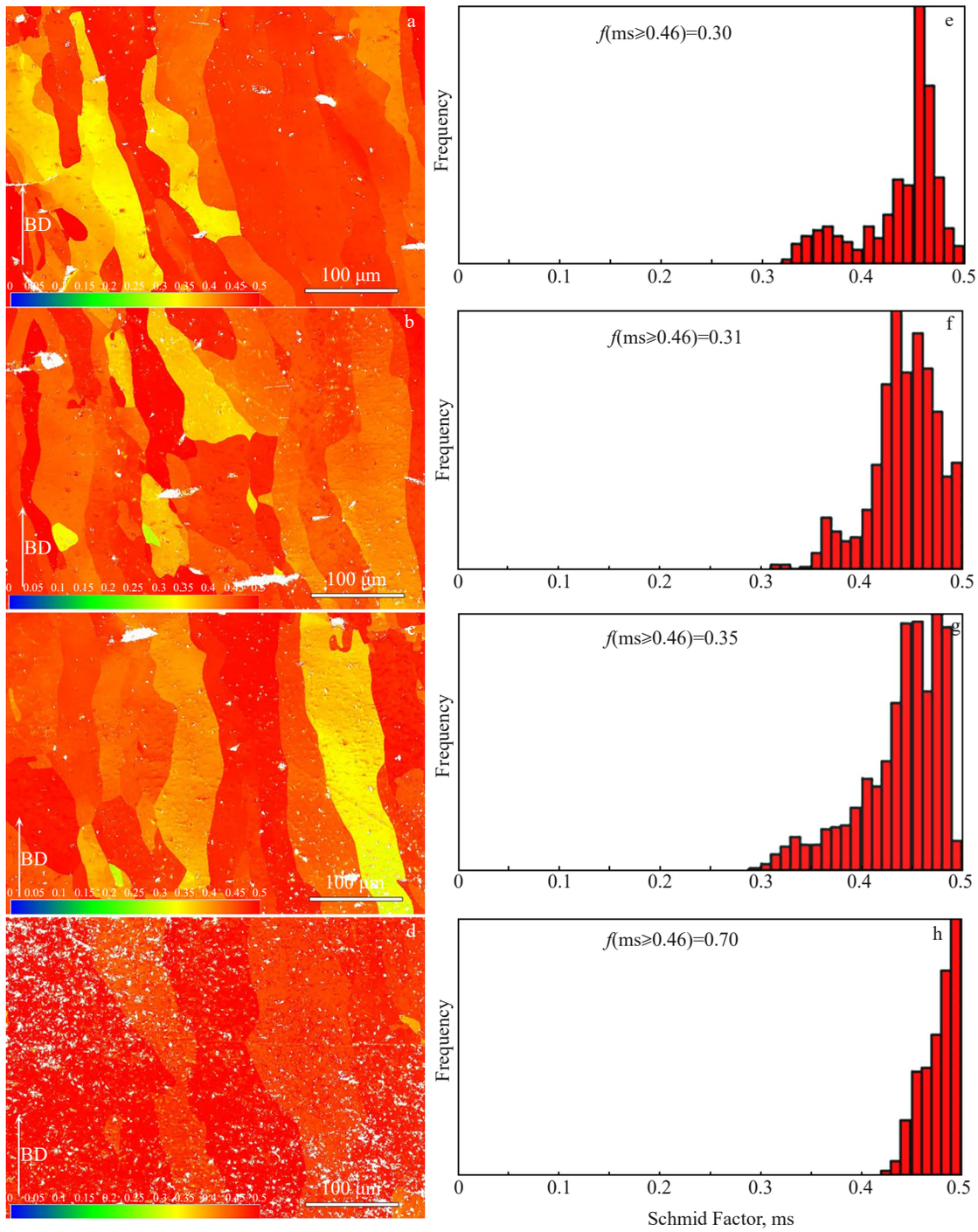

Fig.12 Schmid factor distributions of Ta specimens after SLM process with single-layer scanning at different energy densities: (a, e) 246 J/mm^3, (b, f) 320 J/mm^3, (c, g) 457 J/mm^3, and (d, h) 640 J/mm^3

further increase the microhardness, compared with those after single-layer scanning at the same energy density. The maximum microhardness of Ta specimen is 2307 MPa. This is because the increase in energy density raises the dislocation density of SLM-processed Ta. Therefore, the dislocation slip requires more energy to simultaneously move the numerous dislocations under the same compressive stress, i. e., the deformation is hindered and the strength is enhanced. Besides, each newly formed layer of Ta specimen during double-layer scanning remelts the previously formed layer, resulting in finer grain size (Fig.8), more grain boundary area, and higher intensity at the grain boundaries (compared with that in the grain). Thus, the microhardness of Ta specimens after SLM process with double-layer scanning is further improved.

Fig. 14 shows the ultimate tensile properties of Ta specimens after different SLM processes. The ultimate tensile strength and elongation are increased with increasing the energy density. The double-layer scanning strategy improves

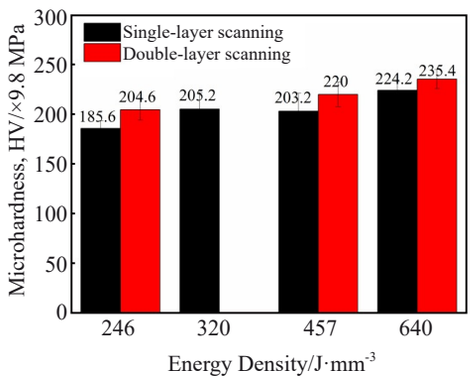

Fig.13 Microhardness of Ta specimens after different SLM processes

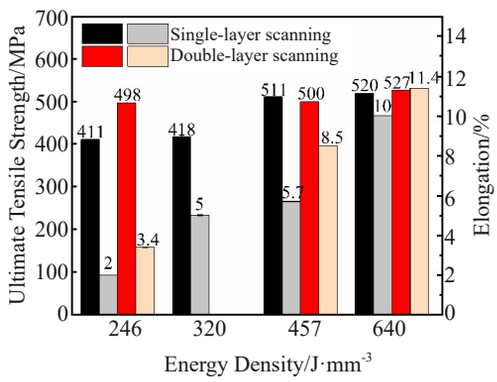

Fig.14 Ultimate tensile strength and elongation of Ta specimens after different SLM processes

the strength and greatly increases the elongation at the same time. The maximum ultimate tensile strength and elongation is 527 MPa and 11.4% for the Ta specimen after SLM process with double-layer scanning at 640 J/mm^3, respectively. This is mainly due to the increased energy density of a single pass during SLM process. In addition, the dislocation density is increased with increasing the energy density, which increases the resistance to deformation and improves the material strength. At higher energy density (640 J/mm^3), the average Schmid factor of Ta specimens is greater, leading to easy occurrence of slip deformation during tension process and decreasing the damage to the plasticity caused by stress concentration. In addition, the more uniform Schmid factor distribution results in the more homogeneous specimen during tensile deformation, avoiding crack occurrence when the slip rates of two parts are not synchronized under the same tensile force, and therefore increasing elongation. The double-layer scanning strategy also significantly increases the material plasticity, compared with the single-layer scanning strategy. The comprehensive enhancement in the properties of Ta specimens after SLM process with double-layer scanning is mainly due to the increased relative density, which reduces cracks and increases elongation. Additionally, the double-layer scanning remelts partial melt pool, interrupting the upward grain growth and promoting the grain refinement, which also increases the ultimate tensile strength and elongation of Ta specimens. As a result, compared with single-layer scanning, double-layer scanning can achieve better elongation without the strength loss. The optimal processing parameters are energy density of 640 J/mm^3 and double-layer scanning strategy, which can obtain the SLM-processed Ta specimen with microhardness, ultimate tensile strength, and elongation of 2307 MPa, 527 MPa, and 11.4%, respectively.

The fracture morphologies of Ta specimens after SLM process with single-layer and double-layer scanning at

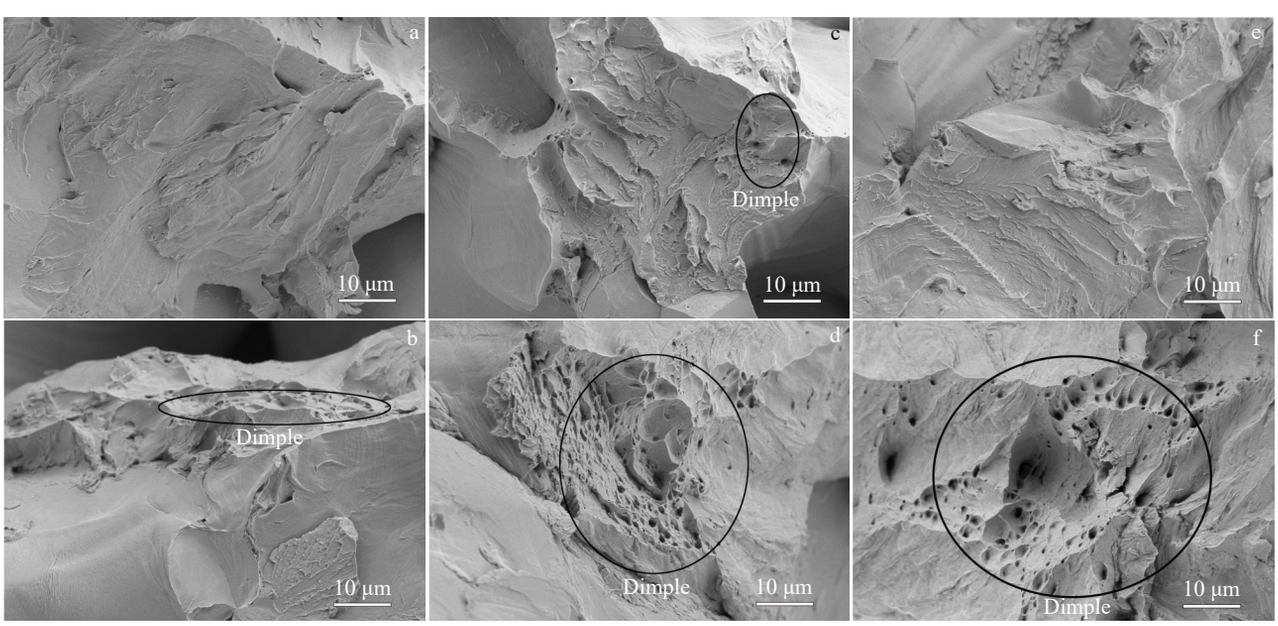

Fig.15 Fracture morphologies of Ta specimens after SLM process with single-layer scanning (a–d) and double-layer scanning (e–f) at different energy densities: (a, e) 246 J/mm^3, (b) 320 J/mm^3, (c) 457 J/mm^3, and (d, f) 640 J/mm^3

different energy densities are shown in Fig.15. At low energy density of 246 J/mm^3, the specimen presents distinct brittle fracture morphology with a ridge-like fracture trend (Fig.15a). At energy densities of 320 – 457 J/mm^3, the fracture morphologies of specimens present the quasi-dissociative fracture, and they have a few dimples as well as a large number of dissociative surfaces. Besides, the fracture morphology still presents the obvious characteristics of brittle fracture (Fig. 15b and 15c). Fig. 15d shows the fracture morphology of Ta specimen after SLM process with single-layer scanning at energy density of 640 J/mm^3. The distinct tough dimples are aggregated in the dissociated section. This phenomenon is consistent with the specimen of high elongation of 10%. The dimples increase after SLM process with double-layer scanning, compared with those after the single-layer scanning, indicating the better plasticity of Ta specimens after double-layer scanning.

3 Conclusions

1) The relative density of Ta specimens after selective laser melting (SLM) is increased to 98.44% with increasing the energy density, and the double-layer scanning process can further increase the relative density of Ta specimen to 98.97%.

2) The microstructure of SLM-processed Ta presents distinct columnar crystal structure, and the double-layer scanning process reduces the size of columnar grains.

3) The microhardness, ultimate tensile strength, and elongation of Ta specimens are increased with increasing the energy density. In addition, compared with single-layer scanning, double-layer scanning can achieve better elongation without the strength loss. The optimal processing parameters are energy density of 640 J/mm^3 and double-layer scanning strategy, which can obtain the SLM-processed Ta specimen with microhardness, ultimate tensile strength, and elongation of 2307 MPa, 527 MPa, and 11.4%, respectively.

References

1 Shahreza B M, Huot J, Antonov M *et al*. *International Journal of Refractory Metals and Hard Materials*[J], 2023, 111: 106 079

2 Li Xu, Zhang Zhibin, He Pengfei *et al*. *Rare Metal Materials and Engineering*[J], 2023, 52(3): 1131 (in Chinese)

3 Luo C Q, Wang C, Wu X D *et al*. *Materials Science and Engineering C*[J], 2021, 129: 112 382

4 Huang G, Pan S T, Qiu J X. *Colloids and Surfaces B: Biointerfaces*[J], 2022, 210: 112 229

5 Guo Y, Chen C, Wang Q B *et al*. *Transactions of Nonferrous Metals Society of China*[J], 2022, 32(9): 2922

6 Yang Kun, Wang Jian, Tang Huiping. *Rare Metal Materials and Engineering*[J], 2022, 51(10): 3922 (in Chinese)

7 Guo Yanhua, Dai Guoqing, Sun Zhonggang *et al*. *Rare Metal Materials and Engineering*[J], 2022, 51(12): 4733 (in Chinese)

8 Alnajjar M, Christien F, Barnier V *et al*. *Corrosion Science*[J], 2020, 168: 108 585

9 Stoll P, Spierings A, Wegener K. *Procedia CIRP*[J], 2020, 168: 108 585

10 Zhang J G, Huang D Y, Hu F L *et al*. *Rare Metal Materials and Engineering*[J], 2022, 51(10): 3619

11 Nicoletto G. *International Journal of Fatigue*[J], 2019, 128: 105 211

12 Xiong Y Z, Gao R N, Zhan H *et al*. *Journal of the Mechanical Behavior of Biomedical Materials*[J], 2020, 104: 103 673

13 Mao B Y, Liu Y, Ye J W *et al*. *Rare Metal Materials and Engineering*[J], 2023, 52(3): 860

14 Sungail C, Abid A D. *Metal Powder Report*[J], 2020, 75(1): 28

15 Zhou L B, Yuan T C, Li R D *et al*. *Materials Science and Engineering A*[J], 2017, 707(7): 443

16 Livescu V, Knapp C M, Gray G T *et al*. *Materialia*[J], 2018, 1: 15

17 Thijs L, Sistiaga M L M, Wauthle R *et al*. *Acta Materialia*[J], 2020, 168: 108 585

18 Liu B, Li B Q, Li Z H. *Results in Physics*[J], 2019, 12: 982

19 Pan L, Zhang C L, Liang H Y *et al*. *Materials Research Express*[J], 2020, 7(5): 56 503

20 Tan C, Shi Q, Li K F *et al*. *International Journal of Refractory Metals and Hard Materials*[J], 2023, 110: 106 008

21 Wei P, Wei Z G, Zhen C *et al*. *Applied Physics A*[J], 2017, 123(8): 540

22 Kurz W, Bezençon C, Gäumann M. *Science and Technology of Advanced Materials*[J], 2001, 2(1): 185

23 Wang J, Pan Z X, Wang Y F *et al*. *Additive Manufacturing*[J], 2020, 34: 101 240

24 Wu B T, Pan Z X, Ding D H *et al*. *Additive Manufacturing*[J], 2018, 23: 151

25 Wang G, Ouyang H, Fan C *et al*. *Materials Research Letters*[J], 2020, 8(8): 283

26 Gorsse S, Hutchinson C, Goune M *et al*. *Science and Technology of Advanced Materials*[J], 2017, 18(1): 584

27 Mughrabi H. *Acta Metallurgica*[J], 1983, 31(9): 1367

28 Liu L F, Ding Q Q, Zhong Y *et al*. *Materials Today*[J], 2018, 21(4): 354

激光工艺参数对选区激光熔化钽微观组织和力学性能的影响

秦　奉[1,2,3,4]，申正焱[2,3,4]，施　麒[2,3,4]，周　舸[1]，姚　岛[5]，赵宇敏[1,2,3,4]，刘　辛[2,3,4]，陈立佳[1]

(1. 沈阳工业大学 材料科学与工程学院，辽宁 沈阳 110870)

(2. 广东省科学院 新材料研究所，广东 广州 510650)

(3. 广东省金属强韧化技术与应用重点实验室，广东 广州 510650)

(4. 国家钛及稀有金属粉末冶金工程技术研究中心，广东 广州 510650)

(5. 河源市省科院研究院，广东 河源 517000)

摘　要：研究了单、双层扫描策略和能量密度（246~640 J/mm^3）对选区激光熔化钽显微组织及力学性能的影响。采用扫描电子显微镜和电子背散射衍射对选区激光熔化钽的显微组织进行表征，并对其显微硬度和拉伸性能进行检测。结果表明，选区激光熔化钽显微组织由明显向上生长的柱状晶构成，双层扫描后的钽具有更细的晶粒尺寸。随着输入能量密度的提高，选区激光熔化钽的强度、显微硬度和塑性均具有明显的上升趋势。此外，双层扫描工艺可进一步提高材料密度，且在保留强度的基础上，增强材料塑性。在能量密度为640 J/mm^3（双层扫描）时，金属钽性能最优，显微硬度、极限抗拉伸强度及延伸率分别为2307 MPa，527 MPa和11.4%。

关键词：选区激光熔化；扫描策略；力学性能；钽

作者简介：秦　奉，女，1996年生，博士生，沈阳工业大学材料科学与工程学院，辽宁 沈阳 110870，E-mail：1090070721@qq.com